Classical Density Functional Study of Wetting Transitions on Nanopatterned Surfaces

P. Yatsyshin[1], A. O. Parry[2], C. Rascón[3], and S. Kalliadasis[1]

[1] Department of Chemical Engineering
[2] Department of Mathematics
Imperial College London, London, SW7 2AZ, United Kingdom
[3] GISC, Department of Mathematics, Universidad Carlos III de Madrid, 28911 Leganés (Madrid), Spain

E-mail: p.yatsyshin@imperial.ac.uk

Abstract.

Even simple fluids on simple substrates can exhibit very rich surface phase behaviour. To illustrate this, we consider fluid adsorption on a planar wall chemically patterned with a deep stripe of a different material. In this system, two phase transitions compete: *unbending* and *pre-wetting*. Using microscopic density-functional theory, we show that, for thin stripes, the lines of these two phase transitions may merge, leading to a new two-dimensional–like wetting transition occurring along the walls. The influence of intermolecular forces and interfacial fluctuations on this phase transition and at complete pre-wetting are considered in detail.

PACS numbers: 31.15.-p, 05.20.Jj, 68.08.Bc, 68.18.Jk

Submitted to: *J. Phys.: Condens. Matter*

1. Introduction

Interest in wetting and adsorption on patterned surfaces has been rapidly growing over the last few decades, across different theoretical, experimental and applied fields of study [1–7]. Wetting and interfacial phenomena are dominated by the rich interplay between intermolecular forces and the fluctuation effects associated with thermal noise and interfacial capillary waves [8–12]. These lead to a very rich picture of possible surface phase behaviour occurring over different length-scales, that call for cross-disciplinary fundamental investigations. Surface effects are also highly relevant to nucleation [13–16], droplet formation and growth [17, 18], vapour–liquid–solid growth of nanowires [19, 20], and burgeoning laboratory-on-a-chip technologies.

In the present work, we consider fluid adsorption on a planar wall chemically decorated with a stripe of a stronger adsorbing material. We suppose that both materials (the wall's and the stripe's) undergo first-order wetting transitions when they form homogeneous planar substrates with wetting temperatures $T_{\rm w}^{(\rm w)}$ and $T_{\rm w}^{(\rm s)} < T_{\rm w}^{(\rm w)}$ for the outer wall (w) and the stripe (s), respectively. Earlier studies based mainly on phenomenological interfacial models have shown that the stripe may induce a first-order *unbending* transition, where the local adsorption near the stripe jumps between two microscopic values [21–24]. Heuristically, this transition is associated with the flattening of the local height of the liquid–gas interface pinned to the wall, which also occurs on homogeneous but non-planar substrates [25], and is closely related to the change from Wenzel to Cassie–Baxter states on rough surfaces. What was not appreciated in these earlier studies was how the pre-wetting transition is modified on patterned surfaces. For example, in the studies of Bauer et al. [21, 23], the pre-wetting properties of the outer wall were not considered. More specifically, the binding potential for the outer wall was only considered to have a single minimum in order to model complete wetting as simply as possibly. In addition, the potential of the stripe phase was chosen to be weaker, so that the wetting temperature is higher than that of the outer wall. In the present study we consider a different scenario where both the outer wall and stripe phase exhibits first-order wetting transitions with the wetting temperature of the stripe being lower. As we shall see this considerably enriches the phase diagram because of the interplay between unbending and complete pre-wetting. The possibility of complete pre-wetting was first pointed out by Saam [5] that a step on a substrate may nucleate a layer of the thicker pre-wetting film. As the pre-wetting transition is approached, this layer grows laterally along the wall, analogous to two-dimensional (2D) complete wetting. Such *complete pre-wetting* has subsequently been observed in microscopic classical density functional theory (DFT) studies of fluid adsorption in capped capillaries, wedges and chemically patterned walls [26].

Classical DFT has long been used as a theoretical tool for studying the phase transitions of inhomogeneous fluids from a microscopic perspective. A systematic construction of the classical equilibrium DFT formalism, along with a review of the earlier literature can be found in the articles by Evans [27, 28]. A comprehensive and

modern review of classical DFT, along with a valuable extension of the equilibrium formalism to non-equilibrium systems is given by Lutsko [29]. Also noteworthy are the reviews by Wu [30] and Lander *et al.* [31], which focus on the applications of the theory to numerous problems in colloidal, polymer and solid matter physics. As far as computational developments for classical DFT are concerned, these go back to early works on obtaining the density of fluids in confinement in both 2D and three-dimensional geometries (e.g. [35, 36]). But in the present decade, the explosive growth of available computational power and especially the development of sophisticated numerical methodologies [32–34], have provided the necessary tools to perform detailed numerical parametric studies employing classical DFT in problems of wetting. Earlier studies of adsorption mainly focused on planar walls and infinite capillary slits and pores. In this study, we adopt a classical DFT model to study global phase diagrams for fluid adsorption on a surface with a chemical stripe and, in particular, investigate the interplay between the unbending transition and the (complete) pre-wetting transition. We will show that, for sufficiently narrow stripes, the line of unbending transitions may merge with the pre-wetting line. When this occurs, one may induce another 2D wetting transition along the surface, which is first-order in character in the present mean-field study. Fluctuation effects at this transition, and also at complete pre-wetting, are discussed in detail.

2. Classical density functional theory

Within the frame of classical DFT, the equilibrium one-body density distribution $\rho(\mathbf{r})$ may be obtained by minimising the grand free-energy functional [27–31]:

$$\Omega[\rho(\mathbf{r})] = F[\rho(\mathbf{r})] - \int \mathrm{d}\mathbf{r}\, \rho(\mathbf{r})\,(\mu - V(\mathbf{r})), \tag{1}$$

where $F[\rho(\mathbf{r})]$ is the intrinsic Helmholtz free energy functional, μ is the chemical potential and $V(\mathbf{r})$ is the external potential arising from the cumulative substrate–fluid interactions.

We consider a Van der Waals-like classical DFT model which separates $F[\rho(\mathbf{r})]$ into contributions modelling the repulsive hard-core and the attractive part of the fluid–fluid intermolecular potential. To this end, we write:

$$\begin{aligned} F[\rho(\mathbf{r})] &= \int \mathrm{d}\mathbf{r}\; [\, f_{\mathrm{id}}(\rho(\mathbf{r})) + \rho(\mathbf{r})\,\psi(\rho(\mathbf{r}))\,] \\ &\quad + \frac{1}{2}\int \mathrm{d}\mathbf{r} \int \mathrm{d}\mathbf{r}'\; \rho(\mathbf{r})\,\rho(\mathbf{r}')\,\varphi_{\mathrm{attr}}(|\mathbf{r}-\mathbf{r}'|), \end{aligned} \tag{2}$$

where $f_{\mathrm{id}}(\rho) = k_{\mathrm{B}}T\rho(\ln(\lambda^3\rho) - 1)$ is the ideal free energy density, and λ is the thermal wavelength. The first (integral) term in (2) is the standard local approximation to the repulsive contribution to the free energy; $\psi(\rho)$ is the free energy density of a bulk hard sphere fluid, for which we use the Carnahan–Starling equation of state:

$$\psi(\rho) = k_{\mathrm{B}}T\,\frac{\eta(4-3\eta)}{(1-\eta)^2}, \qquad \eta = \pi\sigma^3\rho/6, \tag{3}$$

where σ is the hard sphere diameter. The second term in (2) is the standard mean-field treatment of the attractive part of the intermolecular potential $\varphi_{\text{attr}}(r)$. In our study, we consider systems with long-ranged dispersion interactions modelled by

$$\varphi_{\text{attr}}(r) = \begin{cases} 0, & r \le \sigma \\ \varphi^{\text{LJ}}_{\sigma,\varepsilon}(r), & r > \sigma, \end{cases} \tag{4}$$

where $\varphi^{\text{LJ}}_{\sigma_0,\varepsilon_0}$ is the Lennard-Jones (LJ) potential:

$$\varphi^{\text{LJ}}_{\sigma_0,\varepsilon_0}(r) = 4\varepsilon_0 \left[\left(\frac{\sigma_0}{r}\right)^{12} - \left(\frac{\sigma_0}{r}\right)^{6} \right]. \tag{5}$$

In what follows, we choose the system of units, where the hard-core diameter σ and the well depth ε of the fluid–fluid LJ interactions are set as units of length and energy, respectively.

The cumulative external potential $V(\mathbf{r}) \equiv V_L(\mathbf{r})$ of a wall decorated by a macroscopically deep stripe of width L is obtained by integrating the pairwise substrate–fluid potentials over the volumes occupied by both materials. These potentials are also given by (5), but with the material-specific parameters: ε_{w}, σ_{w} and ε_{s}, σ_{s} for the wall and stripe materials, respectively. To avoid a non-physical divergence of $V_L(\mathbf{r})$, at contact with the fluid, and to reduce the fluid–substrate repulsions [which are not adequately captured by (2)], as a purely mathematical device, we suppose that the substrate surface in contact with the fluid is coated by a thin layer of an inert solid phase of width H_0. For Cartesian coordinates, with the origin at the center of the stripe, y the distance normal to the wall, and the x-axis aligned with the wall perpendicularly to the stripe, the potential of the stripe $V_L(x,y)$ can be obtained from the standard "3–9" potential of a homogeneous LJ wall ($L = 0$). The latter is given by [34]:

$$V_0(y) = 4\pi\rho_{\text{w}}\varepsilon_{\text{w}}\sigma_{\text{s}}^3 \left[-\frac{1}{6}\left(\frac{\sigma_{\text{w}}}{H_0+y}\right)^3 + \frac{1}{45}\left(\frac{\sigma_{\text{w}}}{H_0+y}\right)^9 \right], \tag{6}$$

where ρ_{w} is the average density of the substrate material. The potential $V_L(x,y)$ of a striped wall can then be expressed as

$$V_L(x,y) = V_0(y) - \rho_{\text{w}} \int_{\nu_L} \mathrm{d}\mathbf{r}'\, \varphi^{\text{LJ}}_{\sigma_{\text{w}},\varepsilon_{\text{w}}}(|\mathbf{r}-\mathbf{r}'|) + \rho_{\text{s}} \int_{\nu_L} \mathrm{d}\mathbf{r}'\, \varphi^{\text{LJ}}_{\sigma_{\text{s}},\varepsilon_{\text{s}}}(|\mathbf{r}-\mathbf{r}'|), \tag{7}$$

where the integration is carried out over the volume ν_L of the stripe, excluding the coating: $\nu_L = \{(x,y,z) : -L/2 \le x \le L/2, -\infty < y \le -H_0, -\infty < z < \infty\}$. With this choice of potential, the equilibrium profile $\rho(\mathbf{r}) = \rho_L(x,y)$, where again y is the distance normal to the wall.

Although the present classical DFT model (2) describes the intermolecular attractions in a non-local mean-field fashion, which allows us to consider stripes as narrow as several hard-core diameters, the intermolecular repulsions are treated by a purely local approximation, which neglects the excluded volume correlations. As a result, the density profiles we compute do not exhibit the characteristic near-wall oscillations and layering, which can be captured with more refined non-local

approximations, such as weighted density or fundamental measure theories [35–37]. However, we do not expect the molecular packing effects to be important for the qualitative aspects of wetting by liquid above the fluid bulk triple point, because layering transitions typically do not interfere with pre-wetting. Similarly, the mean-field nature of the model energy functional (2) implies that our results do not capture effects associated with capillary wave fluctuations. However, we expect these to be unimportant for all practical purposes in the transitions considered here, as discussed later. With these shortcomings, the model functional (1) – (4) provides a suitable microscopic starting point to study the interplay between unbending and pre-wetting on a striped substrate. Further discussion of the physical approximations underlying (1) – (4) and possible approaches to their numerical solution can be found elsewhere, e.g., in references [26, 32, 34, 38, 39].

3. Wetting phenomenology

Recall that we have chosen the hard-core diameter σ and the well depth ε of the fluid–fluid LJ interactions as the units of length and energy, respectively. The units of temperature are then given by $\varepsilon/k_{\rm B}$, and the bulk critical temperature is $T_{\rm c} \approx 1.006$. We further suppose that $\rho_{\rm w} = \rho_{\rm s} = 1$ in (7), and fix the parameters of the LJ fluid–substrate potentials as $\varepsilon_{\rm w} = 0.6$, $\varepsilon_{\rm s} = 1$, $\sigma_{\rm w} = \sigma_{\rm s} = 2$, with the shifting parameter $H_0 = 5$ in (6) and (7).

3.1. Pre-wetting and complete pre-wetting

3.1.1. Pre-wetting

We first obtain the wetting phase diagram for flat substrates made purely of the same material as the wall (w), or that of the stripe (s) [5]. To this end, we have computed the adsorption Γ_0, which can be obtained from the density profiles $\rho(\mathbf{r}) \equiv \rho(y)$ [32, 34]:

$$\Gamma_0 = \int_0^\infty dy \, [\, \rho(y) - \rho_{\rm b} \,], \tag{8}$$

where $\rho_{\rm b}$ is the bulk fluid density; for very thick films, Γ_0 is proportional to the thickness of the adsorbed wetting layer. A first-order wetting transition refers to the discontinuous divergence of Γ_0 at the wetting temperature $T_{\rm w}$ and bulk saturation chemical potential $\mu_{\rm sat}(T)$. Associated with this transition, there is a line of thin–thick transitions, where the jump in Γ_0 is finite, occurring off bulk coexistence, referred to as pre-wetting. Figure 1(a) shows a plot of the coexisting adsorptions as we move along the pre-wetting lines of both materials. The maximum of each curve corresponds to the pre-wetting critical point at which thin–thick coexistence ends [1, 5, 40]. The divergence of the thicker film adsorption near $T_{\rm w}$ is controlled by the long-range tails of the intermolecular forces. In the case of the LJ forces, we have for the thick coexisting film: $\Gamma_0 \propto (T - T_{\rm w})^{-1/2}$ for $T \to T_{\rm w}$ [39, 40].

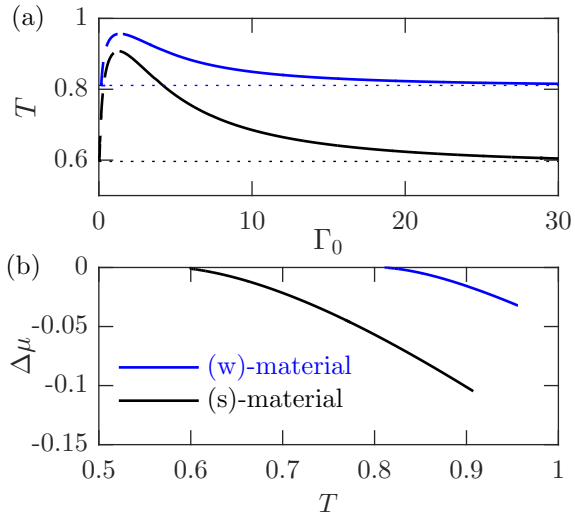

Figure 1. Pre-wetting transitions for planar substrates made of one type of material only: that of the wall (w) (blue lines) and that of the stripe (s) (black lines). Figure (a) shows the binodals, that is, the coexisting adsorptions along the respective pre-wetting lines. Horizontal asymptotes of the diverging thick film adsorption are drawn at the respective wetting temperatures $T_{\mathrm{w}}^{(\mathrm{i})}$. Figure (b) is the phase diagram in the $T-\Delta\mu$ plane. The respective wetting temperatures are $T_{\mathrm{w}}^{(\mathrm{w})} \approx 0.81$ and $T_{\mathrm{w}}^{(\mathrm{s})} \approx 0.60$.

The computed pre-wetting lines in the T–μ plane are shown in figure 1(b), where $\Delta\mu = \mu - \mu_{\mathrm{sat}}$ is the deviation from the saturation chemical potential. Note that these pre-wetting lines lay in the gas region of the bulk phase diagram ($\Delta\mu < 0$), and approach bulk coexistence tangentially at the respective $T_{\mathrm{w}}^{(\mathrm{i})}$, i = w, s. As expected, the deeper well of the fluid–stripe LJ interaction leads to $T_{\mathrm{w}}^{(\mathrm{s})} < T_{\mathrm{w}}^{(\mathrm{w})}$, and a more pronounced pre-wetting line $\mu_{\mathrm{pw}}^{(\mathrm{s})}(T)$, which extends deeper into the gas region. Near the respective wetting temperatures $T_{\mathrm{w}}^{(\mathrm{i})}$, the pre-wetting lines are described by their asymptotic behaviour, which follows from analysis of the Clausius–Clapeyron equation [5, 34, 41]: $\mu_{\mathrm{sat}} - \mu_{\mathrm{pw}}^{(\mathrm{i})}(T) \propto \left(T - T_{\mathrm{w}}^{(\mathrm{i})}\right)^{3/2}$.

3.1.2. Complete pre-wetting

The phenomenon of wetting takes place when one of the coexisting phases of a fluid (gas or liquid) is preferentially adsorbed near a wall (or third phase). If, for example, liquid is preferred, a liquid layer is formed at the wall–gas interface, whose thickness increases as the pressure, say, is increased towards liquid–gas coexistence. When the contact angle is zero, this intruding layer of liquid is macroscopically large, and we say that the liquid completely wets the wall.

An analogous phenomenon may occur *along* a wall when one of the coexisting phases (thin or thick) associated with pre-wetting is preferentially adsorbed at an inhomogeneity (for example, a step or a chemical stripe). Then, as the pre-wetting coexistence is approached, a macroscopically large layer of the, say, thick phase may intrude between the inhomogeneity and the coexisting thin phase which is stable far

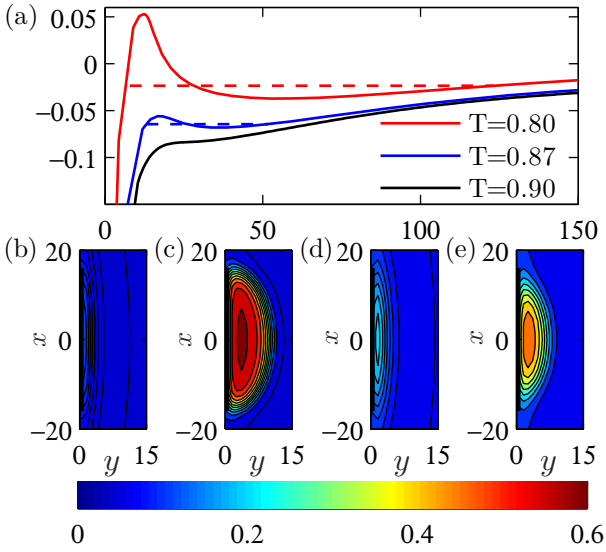

Figure 2. Adsorption isotherms on a wall with a stripe of width $L = 32$ at three different temperatures (a). At the two lower temperatures unbending transitions occur at chemical potentials $\mu_u(T)$: $\Delta\mu_u(0.80) \approx -0.0236$ and $\Delta\mu_u(0.87) \approx -0.0645$, as determined by the equal area constructions (dashed lines). The isotherm at $T = 0.90$ lies above the unbending critical temperature. Density profiles for the coexisting phases at $T = 0.8$ [(b) and (c)] and $T = 0.87$ [(d) and (e)].

from it. This phenomenon, referred to as *complete pre-wetting*, was originally speculated by Saam for a stepped surface [5], and has been subsequently observed in microscopic classical DFT studies for a number of other systems [26, 34].

3.2. Unbending

Another phase transition that may occur on a patterned or sculpted substrate is *unbending*. This phase transition corresponds to a local condensation of liquid driven by the competition between attractive substrate–fluid forces and the effect of the liquid–gas surface tension. This phenomenon was first described for a corrugated wall, in which the troughs discontinuously fill with liquid below the wetting temperature, thereby flattening the liquid–gas interface (hence, the name *unbending*) [25]. Similar phenomena were studied on chemically patterned substrates, including stripes and arrays of stripes [24].

Unbending may occur even for walls that show critical wetting, where no pre-wetting transitions exist. However, for walls that exhibit first-order wetting, unbending may act as a nucleation site that triggers complete pre-wetting occurring along the substrate. The interplay between these transitions is studied here.

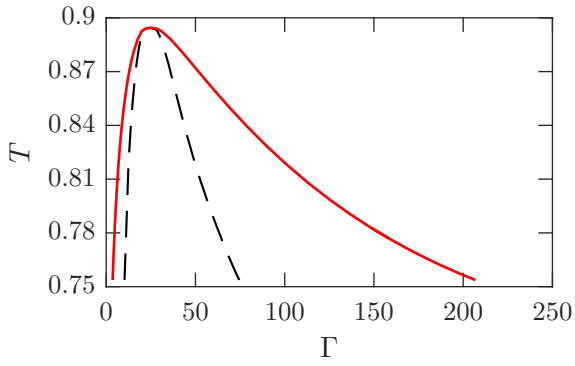

Figure 3. Binodal of the unbending transition on a wall decorated with a stripe of width $L = 32$. The loci of transitions and spinodals are plotted as solid red and dashed black curves, respectively.

4. Results

In order to study phase coexistence at a decorated wall, we introduce the excess adsorption relatively to a homogeneous planar wall:

$$\Gamma = \int_{-\infty}^{\infty} dx \int_{0}^{\infty} dy \, \left[\rho_L \left(x, y \right) - \rho^{(\mathrm{w})} \left(y \right) \right], \tag{9}$$

where $\rho_L \left(x, y \right)$ is the fluid density on the decorated wall, and $\rho^{(\mathrm{w})} \left(y \right) (= \rho_{L=0}(x, y))$ is the equilibrium density profile in the absence of the stripe, computed at the same values of T and μ. At a given temperature, the thermodynamic quantity conjugate to the adsorption Γ is the excess grand potential Ω_{ex} [26, 34]:

$$\Omega_{\mathrm{ex}} = \Omega \left[\rho_L \left(x, y \right) \right] - \Omega \left[\rho^{(\mathrm{w})} \left(x \right) \right]. \tag{10}$$

which is related to Γ by:

$$\Gamma \left(\mu \right) = -\frac{1}{\mathcal{L}} \left(\frac{\partial \Omega_{\mathrm{ex}}}{\partial \mu} \right)_T, \tag{11}$$

where $\mathcal{L}$ is the transverse dimension of the system along the z-axis. Following a standard Maxwell construction, this expression may be used to determine phase coexistence by applying an equal areas construction to the adsorption isotherm $\Gamma \left(\mu \right)$, which corresponds to the equality of the excess grand potentials [42]. Therefore, by computing isotherms on a striped wall at different values of T, we can, in principle, obtain the full picture of the surface phase coexistence.

4.1. Unbending

First, we present results for the unbending transition occurring near a stripe of width $L = 32$. Figure 2 shows adsorption isotherms at three different temperatures. At the two lower temperatures, an equal areas construction determines the coexisting adsorptions at the unbending transition. For the highest temperature $T = 0.9$, there

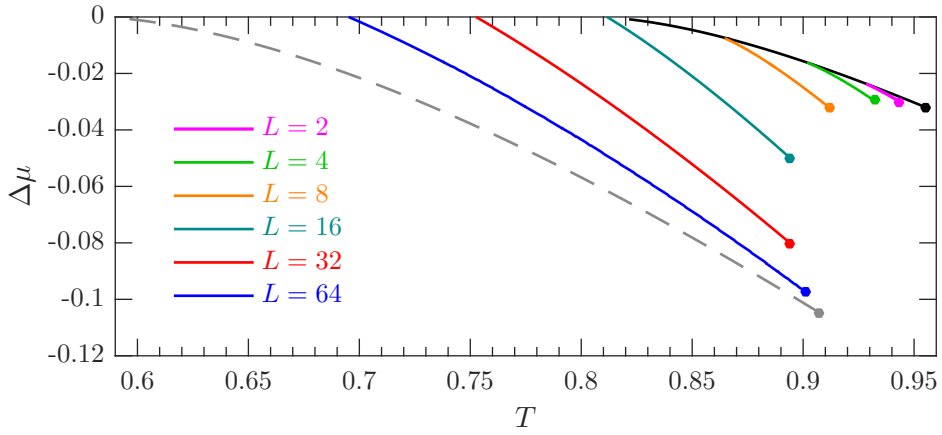

Figure 4. Unbending lines in the T–μ plane for stripes of different widths. The pre-wetting lines for the pure wall material (solid black line) and for the pure stripe material (dashed grey line) are also shown. For narrow stripes, $L = 8$, 4 and 2, the unbending line meets the black pre-wetting line tangentially at temperatures $T^* \approx 0.865$, 0.902 and 0.928, respectively.

is no Van der Waals loop, signalling that this isotherm is above the unbending critical temperature. Density profiles of the two coexisting phases at the lowest temperature $T = 0.8$ (where the loop is most pronounced) are also shown. The binodal for this system is represented in figure 3, showing the temperature dependence of the excess adsorptions Γ of the coexisting phases along the whole unbending line. In the T–$\Delta\mu$ plane, this unbending line (red curve in figure 4) joins the liquid–gas coexistence line at a temperature $T \approx 0.75$, and extends away from coexistence ending at an unbending critical point at $T \approx 0.89$. Note that the unbending line does not meet the liquid–gas coexistence curve tangentially since the difference in the coexisting adsorptions at that point remains finite (see figure 3).

Repeating this methodology, we have determined the locations of the unbending lines for a variety of stripe widths from $L = 64$ to $L = 2$. The results are shown in figure 4. For the largest width $L = 64$, the unbending line lies close to the pre-wetting line of a homogeneous substrate made entirely of the material (s) (shown as the dashed grey curve). This is consistent with earlier predictions based on simple effective interfacial Hamiltonian models [24]. As the stripe width is reduced, so the unbending line moves towards the pre-wetting line of the homogeneous outer wall (w) (black curve). For $L = 64$, 32 and 16, the unbending lines are separate from this latter pre-wetting line. However, for $L = 8$, 4 and 2, it merges with the pre-wetting line at temperatures $T^* \approx 0.87$, 0.9 and 0.93, respectively. Our numerics are consistent with the expectation that, for these cases, the unbending line merges tangentially with the pre-wetting line.

Beyond the present mean-field classical DFT study, we can anticipate that fluctuations round any first-order unbending transition, which will manifest itself as a sharp, but nonetheless continuous, increase in the adsorption. In fact, for large L and close to liquid–gas coexistence, the rounding of the unbending line is of negligible

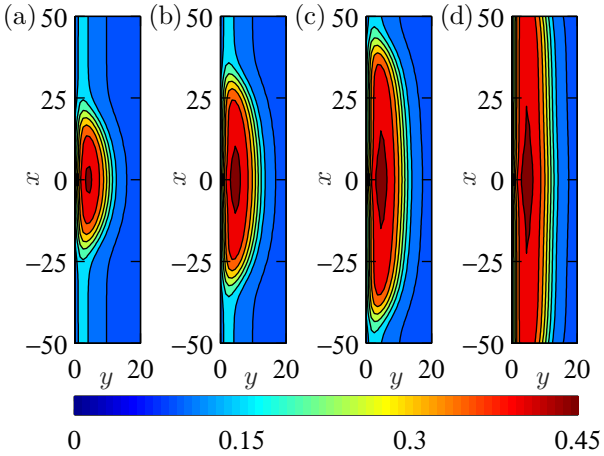

Figure 5. Representative density profiles in the approach to complete pre-wetting for $L = 4$ at $T = 0.92$ ($\Delta\mu_{\rm pw}^{\rm (w)}(0.92) \approx -0.0211$) showing the growth of the lateral extent of the thick pre-wetting layer away from the stripe. The distance to pre-wetting, $\mu - \mu_{\rm pw}^{\rm (w)}(0.92)$, is approximately (a) -1.5×10^{-3}, (b) -4.7×10^{-4}, (c) -1.6×10^{-4}, (d) -9.6×10^{-6}.

practical importance and would not even be seen in simulations, because the difference in adsorptions between the (pseudo) coexisting phases is so large.

4.2. Complete pre-wetting

For the stripes of width $L = 64$, 32 and 16, the substrate shows complete pre-wetting along the entire pre-wetting curve. That is, if we choose an isotherm lying above $T_{\rm w}^{\rm (w)}$ (but below the pre-wetting critical temperature) and increase the chemical potential towards that of pre-wetting $\mu_{\rm pw}(T)$, a layer of the thicker pre-wetting film spreads out laterally along the wall, at each side of the stripe (see figure 5).

The divergence of the adsorption for this transition is very similar to that occurring near a geometrical step, as in the original work of Saam [5]. At large lateral lengths of the adsorbed films, the film growth is determined by the long-range decay of the cumulative potential exerted on the fluid by the slab of material (s) which has the power-law:

$$\int_{\nu_L} {\rm d}\mathbf{r}' \varphi^{\rm LJ}_{\sigma_{\rm s},\varepsilon_{\rm s}}(|\mathbf{r} - \mathbf{r}'|) \sim \frac{1}{x^4}, \tag{12}$$

as $x \to \infty$ and fixed y. It is then clear, making analogy with the influence of intermolecular forces for complete wetting, that the divergence of the adsorption at complete pre-wetting with dispersion forces must follow the power-law [26, 43]:

$$\Gamma(\mu) \propto (\mu_{\rm pw} - \mu)^{-1/4}, \quad \text{as} \quad \mu \to \mu_{\rm pw}. \tag{13}$$

These predictions are altered if the chemical stripe is not of macroscopic depth. In that case, the cumulative potential exerted on a fluid particle far from the stripe decays as x^{-5}, faster than (12). The adsorption in the approach to complete pre-wetting then diverges with a different exponent $\Gamma(\mu) \propto (\mu_{\rm pw} - \mu)^{-1/5}$, instead of (13).

This is another example of using a substrate shape in order to tune the influence of intermolecular forces on the adsorption, and thus to control the adsorption.

4.3. Transverse wetting along pre-wetting

The most striking feature of the phase diagram in figure 4 is the tangential merging of the unbending and pre-wetting lines at $T^* \approx 0.93$, 0.9 and 0.87 observed for narrow stripes ($L = 2$, 4 and 8). In this case, complete pre-wetting is only observed for isotherms that approach $\mu_{\rm pw}(T)$ for temperatures larger than the corresponding T^*. On increasing the chemical potential towards pre-wetting at lower temperatures (in the range $T_{\rm w}^{(\rm w)} < T < T^*$), the adsorption Γ remains finite, implying that only a finite layer of the thicker pre-wetting film spreads laterally away from the stripe. In other words, the stripe is only partially wet by the thicker pre-wetting layer for $T < T^*$, while, for $T > T^*$ it is completely wet. Therefore, crossing the pre-wetting line for $T < T^*$ results in a first-order phase transition similar to pre-wetting on a homogeneous wall, but in one lower dimensions. By contrast, this first-order transition is replaced by continuous complete pre-wetting for $T > T^*$. There is, therefore, a direct analogy between the transition occuring at T^* and a first-order wetting transition, in which the unbending and pre-wetting lines play the role of pre-wetting and liquid–gas coexistence, respectively. This explains our numerical findings that the unbending line meets the pre-wetting line tangentially. An elementary calculation using the Clausius–Clapeyron equation to determine the slope of the unbending line $\mu_{\rm u}(T)$ relative to pre-wetting shows that:

$$\mu_{\rm pw}(T) - \mu_{\rm u}(T) \propto (T - T^*)^{4/3}. \tag{14}$$

where we have used the complete pre-wetting power-law, equation (13), to determine the difference in coexisting adsorptions near T^*.

This picture makes it clear that the transition at T^* along $\mu_{\rm pw}(T)$ is a 2D wetting transition, occurring along (i.e. transverse to) the substrate. The order of this transition deserves some discussion. Within the present mean-field classical DFT study, this wetting transition is certainly first-order in nature, so that the excess adsorption Γ diverges discontinuously. However, capillary-wave like fluctuations in the position of the thick–thin interface along the wall can strongly effect this result (at least, in principle). Recall that, strictly speaking, first-order wetting transitions are not possible in 2D for systems whose effective external potential decays faster than an inverse cube, as the potential (12) does [2]. This means two things: that the transverse wetting temperature T^* is renormalised (lowered from its mean-field value) and that the adsorption ultimately diverges continuously, so $\Gamma \propto (T^* - T)^{-1}$, consistent with Abraham's exact solution of wetting in the 2D Ising model [44]. In this case, the unbending line appears as a rounded transition. However, recent studies of wetting in 2D systems have shown that, if the underlying mean-field transition is strongly first-order, the asymptotic critical regime is extremely small, and that the wetting transition remains effectively first-order [45, 46]. This, we believe, is pertinent to the transverse wetting occurring on the stripe substrate.

In fact, if the transverse wetting temperature T^* is close to the wetting temperature of the substrate $T_{\rm w}^{(\rm w)}$, interfacial fluctuations are strongly suppressed because the line tension of the thick–thin interface is prohibitively large. Only for very narrow stripes, where T^* is close to the pre-wetting critical point, are fluctuation effects of any relevance.

5. Conclusions

In this paper, we have aimed to show that even simple fluids on simply structured substrates may exhibit complex phase behaviour. In the present case of a chemical stripe, the interplay of pre-wetting and unbending transitions means that the decorated surface exhibits not one but two different types of wetting transitions; the usual one, occurring at the wetting temperature of the outer surface (corresponding to the unbinding of the liquid–gas interface away from the wall), and a second transition occurring along the pre-wetting line (corresponding to the unbinding of the thin–thick interface along the wall away from the stripe). The possibility of such transverse wetting transitions, and indeed of complete pre-wetting itself, in other geometries has not been fully appreciated previously.

The present work opens up the possibility of using chemical stripes as building blocks to induce further examples of surface phase transitions; for instance, if the chemical inhomogeneity is made of two linear stripes that meet at an angle (forming a "V"), then the complete pre-wetting transition may be substantially modified, similar to predictions for 2D wedge filling transitions. However, studying these transitions using microscopic classical DFT is numerically challenging because the density profile is fully three dimensional. Combining chemical stripes with steps may allow us to tailor the adsorption properties of a surface, both for practical purposes and also to study fundamental predictions for the properties of confined interfaces.

Acknowledgments

PY is grateful to Dr. Miguel A. Durán-Olivencia from the Chemical Engineering Department of Imperial College London for numerous stimulating discussions. We acknowledge financial support from the Engineering and Physical Sciences Research Council of the UK through Grants No. EP/L027186 and EP/L020564 and by the European Research Council through Advanced Grant No. 247031. C.R. also acknowledges the support of the Spanish *Ministerio de Economía y Competitividad* under grant FIS2015-66523-P.

References

[1] S. Dietrich. Wetting Phenomena. In C. Domb and J. L. Lebowitz, editors, *Phase Transitions and Critical Phenomena*, volume 12, page 2. Academic Press, 1988.

[2] G. Forgacs, R. Lipowsky, and Th. M. Nieuwenhuizen. The Behaviour of Interfaces in Ordered and Disordered Systems. In C. Domb and J. L. Lebowitz, editors, *Phase Transitions and Critical Phenomena*, volume 14, page 135. Academic Press, 1991.

[3] K. Binder. Modelling of Wetting in Restricted Geometries. *Annu. Rev. Mater. Res.*, 38:123, 2008.

[4] D. Bonn, J. Eggers, J. Indekeu, J. Meunier, and E. Rolley. Wetting and Spreading. *Rev. Mod. Phys.*, 81:739, 2009.

[5] W. F. Saam. Wetting, Capillary Condensation and More. *J. Low Temp. Phys.*, 157:77, 2009.

[6] A. Checco, B. M. Ocko, M. Tasinkevych, and S. Dietrich. Stability of Thin Wetting Films on Chemically Nanostructured Surfaces. *Phys. Rev. Lett.*, 109:166101, 2012.

[7] D. Lohse and X. Zhang. Surface Nanobubbles and Nanodroplets. *Rev. Mod. Phys.*, 87:981, 2015.

[8] K. Ragil, J. Meunier, D. Broseta, J. O. Indekeu, and D. Bonn. Experimental Observation of Critical Wetting. *Phys. Rev. Lett.*, 77:1532, 1996.

[9] C. Rascón and A. O. Parry. Geometry-Dominated Fluid Adsorption on Sculpted Solid Substrates. *Nature*, 407:986, 2000.

[10] R. Seeman, M. Brinkman, E. J. Kramer, F. F. Lange, and R. Lipowsky. Wetting Morphologies at Microstructured Surfaces. *Proc. Natl. Acad. Sci. U. S. A.*, 102:1848, 2005.

[11] K. Koga, J. O. Indekeu, and B. Widom. Wetting Transitions of Continuously Varying or Infinite Order from a Mean-Field Density-Functional Theory. *Mol. Phys.*, 109:1297, 2011.

[12] K. Murata and H. Tanaka. Surface-Wetting Effects on the Liquid-Liquid Transition of a Single-Component Molecular Liquid. *Nat. Commun.*, 1:16, 2010.

[13] M. Schick and P. Taborek. Anomalous Nucleation at First-Order Wetting Transitions. *Phys. Rev. B*, 46:7312, 1992.

[14] J. F. Lutsko and M. A. Durán-Olivencia. Classical Nucleation Theory from a Dynamical Approach to Nucleation. *J. Chem. Phys.*, 138:244908, 2013.

[15] J. F. Lutsko and M. A. Durán-Olivencia. A Two-parameter Extension of Classical Nucleation Theory. *J. Phys.: Condens. Matter*, 27:235101, 2015.

[16] M. A. Durán-Olivencia and J. F. Lutsko. Mesoscopic Nucleation Nheory for Confined Systems: A One-parameter Mode. *Phys. Rev. E*, 91:022402, 2015.

[17] L. Bao, Z. Werbiuk, D. Lohse, and X. Zhang. Controlling the Growth Modes of Femtoliter Sessile Droplets Nucleating on Chemically Patterned Surfaces. *J. Phys. Chem. Lett.*, 7:1055, 2016.

[18] X. Zhang, Z. Lu, H. Tan, L. Bao, Y. He, C. Sun, and D. Lohse. Formation of Surface Nanodroplets Under Controlled Flow Conditions. *Proc. Natl. Acad. Sci. U. S. A.*, 112:9253, 2015.

[19] K. W. Schwarz and J. Tersoff. From Droplets to Nanowires: Dynamics of Vapor-Liquid-Solid Growth. *Phys. Rev. Lett.*, 102, 2009.

[20] R. E. Algra, M. A. Verheijen, L.-F. Feiner, G. G. W. Immink, W. J. P. van Enckevort, E. Vlieg, and E. P. A. M. Bakkers. The Role of Surface Energies and Chemical Potential during Nanowire Growth. *Nano Lett.*, 11:1259, 2011.

[21] C. Bauer, S. Dietrich, and A. O. Parry. Morphological Phase Transitions of Thin Fluid Films on Chemically Structured Substrates. *Europhys. Lett.*, 47:474, 1999.

[22] C. Rascón and A. O. Parry. Wetting on Non-planar and Heterogeneous Substrates. *J. Phys. Condens. Matter*, 12:A369, 2000.

[23] C. Bauer and E. Dietrich. Phase Diagram for Morphological Transitions of Wetting Films on Chemically Structured Substrates. *Phys. Rev. E*, 61:1664, 2000.

[24] C. Rascón and A. O. Parry. Surface Phase Diagrams for Wetting on Heterogenous Substrates. *J. Chem. Phys.*, 115:5258, 2001.

[25] C. Rascón, A. O. Parry, and A. Sartori. Wetting at Nonplanar Substrates: Unbending and Unbinding. *Phys. Rev. E*, 59:5697, 1999.

[26] P. Yatsyshin, A. O. Parry, and S. Kalliadasis. Complete Prewetting. *J. Phys.: Condens. Matter*, 28:275001, 2016.

[27] R. Evans. The Nature of the Liquid-Vapour Interface and Other Topics in the Statistical Mechanics of Non-Uniform, Classical Fluids. *Adv. Phys.*, 28:143, 1979.

[28] R. Evans. *Fundamentals of Inhomogeneous Fluids*, chapter Density Functionals in the Theory of Nonuniform Fluids., page 85. Dekker, New York, 1992.

[29] J. F. Lutsko. Recent Developments in Classical Density Functional Theory. In *Adv. Chem. Phys.*, page 1. John Wiley & Sons, 2010.

[30] J. Wu. Density Functional Theory for Chemical Engineering: From Capillarity to Soft Materials. *AIChE J.*, 52:1169, 2006.

[31] J. Landers, J. Yu. Gor, and A. V. Neimark. Density Functional Theory Methods for Characterization of Porous Materials. *Colloid Surface A*, 437:3, 2013.

[32] P. Yatsyshin, N. Savva, and S. Kalliadasis. Spectral Methods for the Equations of Classical Density-Functional Theory: Relaxation Dynamics of Microscopic Films. *J. Chem. Phys.*, 136:124113, 2012.

[33] A. Malijevsky and A. O. Parry. Critical Point Wedge Filling. *Phys. Rev. Lett.*, 110:166101, 2013.

[34] P. Yatsyshin, N. Savva, and S. Kalliadasis. Wetting of Prototypical One- and Two-Dimensional Systems: Thermodynamics and Density Functional Theory. *J. Chem. Phys.*, 142:034708, 2015.

[35] B. Gotzelmann, A. Haase, and S. Dietrich. Structure Factor of Hard Spheres Near a Wall. *Phys. Rev. E*, 53:3456, 1996.

[36] P. Bryk, R. Roth, M. Schoen, and S. Dietrich. Depletion Potentials Near Geometrically Structured Substrates. *Europhys. Lett.*, 63:233, 2003.

[37] R. Roth. Fundamental Measure Theory for Hard-Sphere Mixtures: a Review. *J. Phys.: Condens. Matter*, 22:063102, 2010.

[38] P. Yatsyshin, N. Savva, and S. Kalliadasis. Geometry-Induced Phase Transition in Fluids: Capillary Prewetting. *Phys. Rev. E*, 87:020402(R), 2013.

[39] P. Yatsyshin, N. Savva, and S. Kalliadasis. Density Functional Study of Condensation in Capped Capillaries. *J. Phys.: Condens. Matter*, 27:275104, 2015.

[40] R. Evans and A. O. Parry. Liquids at Interfaces: What Can a Theorist Contribute? *J. Phys. Condens. Matter*, 2:SA 15, 1990.

[41] E. H. Hauge and M. Schick. Continuous and First-Order Wetting Transition From the van der Waals Theory of Fluids. *Phys. Rev. B*, 27:4288, 1983.

[42] R. Evans and U. M. B. Marconi. Phase Equilibria and Solvation Forces for Fluids Confined Between Parallel Walls. *J. Chem. Phys.*, 86:7138, 1987.

[43] A. O. Parry, C. Rascón, N. B. Wilding, and R. Evans. Condensation in a Capped Capillary is a Continuous Critical Phenomenon. *Phys. Rev. Lett.*, 98:226101, 2007.

[44] D. B. Abraham. Solvable Model for a Roughening Transition for a Planar Ising Ferromagnet. *Phys. Rev. Lett.*, 44:1165, 1980.

[45] X.-T. Wu, D. B. Abraham, and J. O. Indekeu. Apparent First-Order Wetting and Anomalous Scaling in the Two-Dimensional Ising Model. *Phys. Rev. Lett.*, 116:046101, 2016.

[46] A. O. Parry and A. Malijevsky. Crossover Scaling of Apparent First-order Wetting in Two-dimensional Systems with Short-ranged Forces. *Phys. Rev. E*, 93:062802, 2016.